INTRODUCTION TO FOURIER PTYCHOGRAPHIC IMAGING FOR 3D TOF CAMERAS

Henrik Lietz, Jörg Eberhardt

University of Applied Sciences Ravensburg-Weingarten, Germany

ABSTRACT

Fourier ptychographic imaging (FPI) extends Fourier domain synthetically by capturing several frequency domain shifted images. In addition to spatial resolution enhancement, FPI allows recovery of a complex light field's phase information. Classical FPI approaches are based on a sequence of two-dimensional intensity images. In this article, we introduce FPI for 3D Time-of-Flight (ToF) cameras to increase its lateral resolving power. We discuss what needs to be considered for an experimental setup and why we recommend an aperture-scanning setup with reflection mode illumination. Simulations illustrate the potential of increasing resolution of PMD camera's low-resolution (LR) amplitude images via FPI.

Index Terms – ToF camera, Fourier ptychography, resolution enhancement, phase retrieval

1. INTRODUCTION

Photonic mixing device (PMD) cameras are suitable for fast and robust three-dimensional image acquisition. They use an inherent amplitude modulated signal to measure running time of light and calculate its travel distance from camera to object scene. Since their first introduction in 1996, they were used mostly for industrial imaging under harsh lighting conditions. Currently, development focuses on miniaturization of such cameras for integration in mobile devices like smartphones and tablets.

Advantageously, they are cost efficient, small in size and have low energy consumption. However, there is a great limitation in low lateral and depth resolution. State of the art, lateral sensor resolution is about 64 x 16 pixels (Ifm O3M151) for outdoor systems and reaches a maximum of 512 x 484 pixels (Microsoft Kinect v2) for indoor systems, which is even less than VGA standard from 1987. Depth resolution is in sub-cm range, mainly depending on measurement distance [1].

Since Zheng et al. introduced Fourier ptychographic microscopy [2] in 2013, FPI has received great attention in 2D image processing's research community. With our research project, we want to extend FPI to a further dimension and increase 3D PMD camera's lateral resolution and depth resolution. This work introduces the idea of combining FPI and phase measuring PMD cameras. Therefore, it discusses what has to be considered for an experimental setup. Simulations promise a significant increase in lateral resolution when nine or more LR intensity images are combined.

2. BACKGROUND

2.1 PMD camera

PMD cameras are assigned to ToF based measurement systems, whose working principle is attributable to Schwarte's patent [3] in 1996. Camera's active light source emits a periodically, amplitude modulated measurement signal that travels back and forth from camera to object

scene. Signal's propagation time enables calculation of object distances. Typically, near-infrared (NIR) emitting light sources like LEDs (light-emitting diodes) or VCSELs (vertical-cavity surface-emitting lasers) are used. Switching them on and off can be assumed as a sinusoidal amplitude modulated measurement signal (see Figure 1).
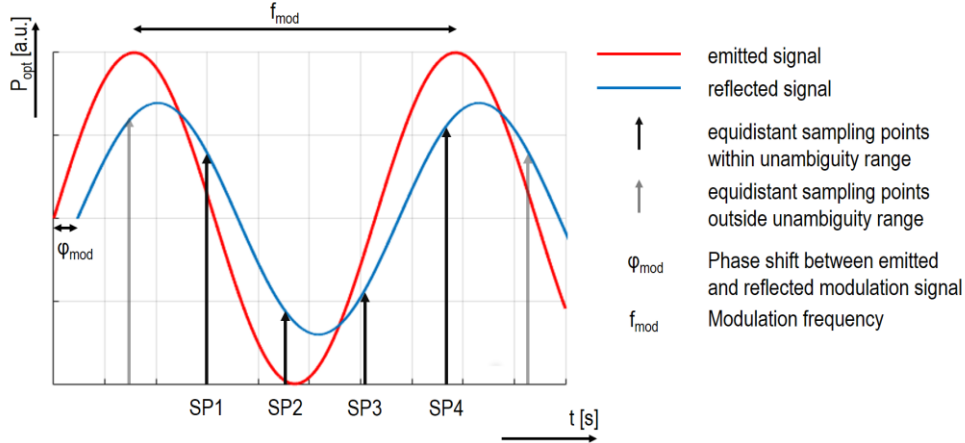

Figure 1: PMD camera's modulation signal is of a sinusoidal shape. Red line is the emitted signal and the blue represents the reflected signal with phase shift φ_{mod}. SP1 to SP4 are equidistant sampling points to recover the reflected signal.

Figure 1 shows two harmonic sine waves, red sine wave represents emitted modulation signal and the blue represents signal reflected from the object scene. Optical losses reduce the reflected signal's amplitude. Phase difference φ_{mod} between both signals is linearly dependent on signal's propagation time and therefore on object distance. It can be reconstructed from four intensity measurements (each is also called a phase image) at temporal equidistant sampling points ($SP1$ to $SP4$) as signal's sinusoidal shape is known. In his dissertation [4], Lange summarizes phase measurement in equation (1).

$$\varphi_{mod} = \mathrm{atan}\left(\frac{SP1-SP3}{SP2-SP4}\right) \qquad (1)$$

Object distance d can be calculated according to equation (2) as phase shift φ_{mod} is measured, modulation frequency f_{mod} is given and light velocity c is known [5]. Because of the periodic modulation signal, distance measurements are only valid within the unambiguous range of 2π.

$$d = \frac{\varphi_{mod} \cdot c}{4\pi \cdot f_{mod}} \qquad (2)$$

PMD sensors output not only distance data but additionally object scene's intensity (amplitude) values. It represents average of phase image's intensity measurements as shown in equation (3).

$$I = \frac{1}{4}\sum_{SP=1}^{4} I(SP) \qquad (3)$$

In summary, PMD cameras are monocular-optical phase measuring systems that record four phase images to output one intensity (amplitude) image and its corresponding distance image at the same time. Periodically modulated signal enables suppression of constant back light [6, 7], which is indispensable, especially for outdoor measurements. PMD cameras allow robust and cost efficient reconstruction of three-dimensional point clouds in real-time under harsh lighting conditions.

2.2 Fourier ptychographic imaging (FPI)

FPI is a computational imaging approach that reconstructs a high-resolution (HR) complex sample image from several LR intensity images [2, 8, 9]. Equation (4) describes a time-independent, complex, monochromatic light field $U(\vec{r})$ in Euler form [10].

$$U(\vec{r}) = A(\vec{r}) \cdot e^{[-i\varphi(\vec{r})]} \qquad (4)$$

Its real amplitude $A(\vec{r})$ and imaginary phase $\varphi(\vec{r})$ depend on the position vector $\vec{r} = (x, y, z)$ in three-dimensional space. To reconstruct the light field $U(\vec{r})$ in a specific object plane (x, y) both, amplitude and phase have to be known. Assuming a constant phase, amplitude can be calculated from intensity measurements according to equation (5).

$$A(\vec{r}) = \sqrt{I(\vec{r})} \qquad (5)$$

However, there is no direct method known to measure phase. Due to light wave's high oscillation frequency, phase can only be determined via the detour of intensity measurements [10]. One representative which reconstructs phase information from intensity measurements is known as phase retrieval. FPI uses an iterative phase retrieval algorithm that estimates complex light field in sample plane, containing its amplitude $A(\vec{r})$ and phase $\varphi(\vec{r})$. It switches between sample's spatial domain (x, y) and Fourier domain (k_x, k_y). Two object constraints assure solution convergence: 1) LR intensity measurements in spatial domain and 2) objective lens' coherent transfer function (CTF) in spatial frequency domain. To estimate the HR complex light field, an initial guess in HR frequency domain is iteratively updated with Fourier transforms (FFT) of each captured LR intensity image from spatial domain. Adjacent input images must overlap > 60 % in Fourier space to ensure convergence. HR intensity and phase images can be output from the recovered complex HR light field. Several authors [2, 8, 9] discuss FPI in more detail.

Figure 2: Classical transmission mode setup for microsopes. FPI is based on LED matrix illumination.

Figure 2 shows a typical FPI setup for two-dimensional microscopy [8]. Spatially coherent light illuminates a thin object from its back under varying angles (k_{xn}, k_{yn}) with plane wavefronts. According to Fraunhofer diffraction, small objects separate the incoming plane wavefront in several diffraction orders in far-field. A camera's lens collects and focusses a limited amount of diffraction orders on the image sensor. Transmitting the 0-order leads to a unique brightness in image plane. Only when at least two diffraction orders (i.e. the 0-order and + 1. or - 1. order) are transmitted, object structures are mapped. The more diffraction orders are transferred, the sharper the image becomes [11]. Therefore, a lens' numerical aperture (NA) defines the achievable image quality (as long as we neglect optical aberrations).

FPI enlarges an optical system's NA synthetically by collecting more diffraction orders than its physical lens does. This is realized by recording an image sequence under varying illumination angles. For example, an image under perpendicular illumination (bright-field illumination) stores low diffraction orders, while increase of illumination angle (dark-field illumination) leads to transmission of higher diffraction orders. Separation of diffraction orders corresponds to shifted frequency band passes (which are limited by the physical lens' NA) in Fourier domain for each input image. In microscopy it is suitable to realize varying illumination angles (and therefore frequency domain shifted images) by using a LED matrix as depicted in Figure 2. The number of input images corresponds to the number of LEDs. Such an illumination mode is limited to thin objects. For thick objects, meaning samples have large extension along the optical axis, one-to-one mapping (from spatial domain to Fourier domain) is invalid as oblique illuminated intensity images will not uniquely map thick sample's frequency spectrum [9].

In summary, FPI estimates a complex light field in an object plane by iteratively superimposing Fourier transforms of LR intensity images in Fourier domain. Two consecutive input images must overlap at least 60 % in spatial frequency domain [12, 13].

3. FPI FOR 3D PMD CAMERAS

Our research project investigates FPI's possibilities to increase image quality of large pixel 3D PMD sensors. In this work, several points which have to be considered for an experimental setup are highlighted. In chapter 5, we will see that simulations promise a significant increase in lateral resolution of PMD camera's intensity images.

Before applying FPI to PMD cameras we want to mention five important points which should be considered for the experimental setup:

- Macroscopic objects: Contrary to microscopic approaches PMD cameras usually capture macroscopic objects which are much bigger than the used wavelength. This reduces diffraction and could affect FPI reconstruction adversely. Macroscopic (thick) objects lead to invalid one-to-one mapping in Fourier domain when using angle-varied illumination. Furthermore, optical rough surfaces may cause speckle which disturbs propagation of diffraction-based directed light.
- Three different types of phase information: Different types of phase information should not be confused with each other. Firstly, PMD camera reconstructs its modulation signal's phase φ_{mod}. This is not directly connected to the second phase information: light field's phase $\varphi(\vec{r})$. This mainly depends on the used wavelength and can be reconstructed by phase-retrieval algorithms. Thirdly, phase information that occurs in spatial frequency domain after Fourier transformation of captured intensity images.
- Inherent light source: According to ToF principle, PMD cameras need to use their inherent light source to reconstruct the modulation signal. Simple use of surrounding light is not possible.
- Reflective mode illumination: Requirement on reflective mode illumination is also reasoned to ToF principle. To capture distance values, running time of light is measured from its emission at the light source to the sample and back to the camera.
- Pixel size: PMD pixels are large in size to ensure reliable separation of their own signal from extraneous light. This limits lateral sensor resolution, especially for outdoor applications where solar spectrum's NIR range causes high amount of backlight.

4. METHODOLOGY

Straightforward implementation of LED matrix configuration (see Figure 2) for PMD cameras is not possible as it is a transmission mode illumination. Reflective mode illumination would require coaxial illumination to avoid blocking imaging beam path with the light source, especially for near-axis illumination. Besides, under angle-varied illumination one-to-one mapping is invalid for thick samples (large extension along the optical axis) [9].

For these reasons, we suggest an aperture-scanning approach adopted from [9] to keep our measurement setup as simple as possible. A plane wavefront hits the object vertically from its front as illustrated in Figure 3. Again, Fraunhofer diffraction leads to a separation in diffraction maxima and diffraction minima. These diffraction orders are collected in far-field at the optical system's aperture stop (Fourier conjugate plane) and limited by its aperture size. Measuring in far-field can be interpreted as light field's Fourier transform [9]. Therefore, the lens' NA naturally serves as a constraint in Fourier domain and limits the transmitted bandpass [9]. Instead of varying illumination angles, the optical system is moved transversally to the optical axis to collect higher diffraction orders in Fourier conjugate plane. By moving the whole camera, several captured LR images could increase transmitted bandpass virtually.
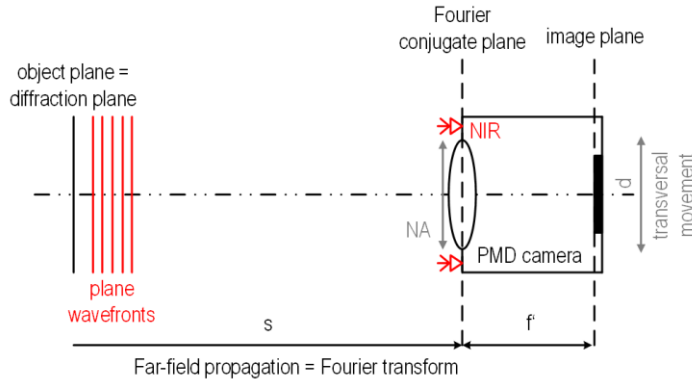
Figure 3: Experimental setup as an aperture-scanning configuration. Reflection mode illumination is required to realize FPI for PMD cameras. Camera's inherent light source emits near-infrared (NIR) radiation. In object plane, plane wavefronts are assumed. Whole camera is transversally scanned to the optical axis.

Our planned experimental setup uses Pmdtechnologies' CamBoard Pico Flexx which emits NIR radiation at 850 nm. It is placed at 1 m distance (s) to sample plane. Temporal coherence is assumed to be fulfilled as the Pico Flexx uses a VCSEL light source. Generally, lasers emit narrow spectral bandwidth light as stimulated emission dominates spontaneous emission. Only a centered region of 30 x 30 pixels of sensor's image field is considered, where a plane wavefront in sample plane is assumed and therefore spatial coherence exists. If necessary, a pinhole can improve requirements for light source's spatial coherence as this mainly depends on the relationship between emitter size and measuring distance. Transversal camera movements are realized by a XY-translation stage. Travel range is about 35 % of the bandpass-limiting NA size to ensure an image overlap of 65 % in Fourier domain. HR reconstruction is based on an FPI algorithm described in the next chapter. For objective evaluation of HR results we recommend the slanted edge method according to [14] which is based on ISO 12233 [15]. Particularly for LR sensors (e.g., outdoor PMD cameras with only 64 x 16 pixels sensor resolution), state-of-the-art evaluation methods of super-resolution algorithms [16, 17] such as standard deviations to a HR ground-truth image are not suitable. Strong discretization by low amount of measurement points (number of pixels) makes the determination of standard deviations error-prone or not possible at all.

5. SIMULATIONS

Simulations are based on two synthetic HR intensity images I, an USAF-1951 and a slanted edge target, both of 120 x 120 pixels size. They are recovered by a LR intensity image sequence of 30 x 30 pixels size. FPI algorithm is based on [8] and can be divided in two main parts:

A. Generation of LR image sequence

1. Approximate amplitude image A from synthetic HR intensity image I: $A = \sqrt{I}$
2. Fast Fourier transformation (FFT) of A: Fourier Spectrum of 120 x 120 pixels
3. Define size of LR images: 30 x 30 pixels
4. Define step factor for consecutive LR image's overlap: $Step\ Factor = 0.35$
5. Calculate optical system's numerical aperture (NA)
6. Set step size of transversal camera movements: $Step\ size = Step\ Factor \cdot \phi_{NA}$
7. Define number of LR images: $N = 3\ x\ 3\ ...\ 9\ x\ 9$
8. Stepwise extraction of N 30 x 30 pixels large frequency ranges from the 120 x 120 pixels large Fourier spectrum which are transversally shifted in steps of step size
9. Inverse FFT to get N LR amplitude images in size of 30 x 30 pixels

Resolving power of the camera's lens is multiple times better than the image sensor's pixel resolution. Therefore, limited bandpass in Fourier space is not of a circled shape (as it is expected from optic's NA). Instead, it is a squared shape of 30 x 30 pixels corresponding to the

considered image sensor size. For this case, step size calculation should be modified according to a rectangular shape with LR image's width/ height as an operand (step 6):

$$Step\ size\ (x) \cong Step\ Factor \cdot LR\ Sensor\ width \qquad (6)$$
$$Step\ size\ (y) \cong Step\ Factor \cdot LR\ Sensor\ height \qquad (7)$$

B. Reconstruction of high-resolution intensity image
  10. Initial guess of HR recovered Fourier space: FFT of an up-sampled LR image grid consisting constant values (e.g., 120 x 120 pixels matrix of ones)
  11. Take a limited frequency range of 30 x 30 pixels from the initial guess Fourier spectrum with the same pixel coordinates like its corresponding LR amplitude image of the generated image sequence
  12. Calculate inverse FFT of the limited frequency range from step 11 to get its corresponding LR amplitude image
  13. Update amplitude image from LR image sequence (same image like in step 9 and 11) with angle information of the one calculated from step 12
  14. FFT the updated amplitude image (from step 13) and add its LR Fourier spectrum to the HR Fourier spectrum recover (at the same pixel coordinates defined in step 11)
  15. Proceed for every further LR image by switching between spatial and spatial frequency domain to update the initial guess of HR Fourier spectrum
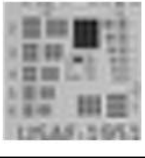 16. Calculate inverse FFT of the final HR Fourier spectrum to achieve reconstructed HR amplitude image.
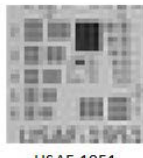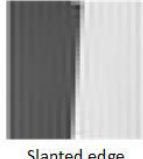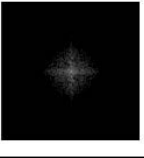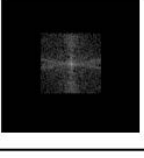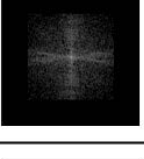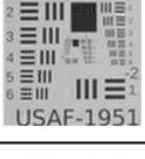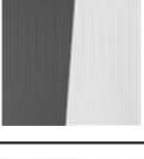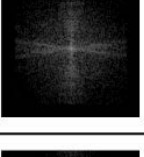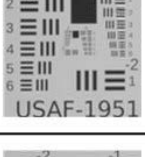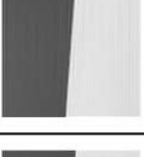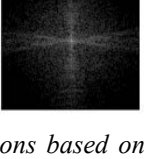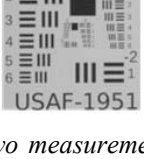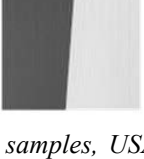
Figure 4: Comparison of FPI simulations based on two measurement samples, USAF-1951 and slanted edge target. LR input images' lateral resolution is increased from 30 x 30 pixels to 120 x 120 pixels for FPI results. From reconstructed HR Fourier space, FPI outputs HR amplitude estimations.

Figure 4 illustrates FPI simulation results for a large pixel digital sensor visualized by two synthetically generated samples. USAF-1951 sample demonstrates resolution enhancement subjectively while slanted edge method allows an objective measurement. On the left, both targets are depicted which has been generated according to simulation part A described above. LR input images shown, are inverse FFT calculations of their ground truth image's centered 30 x 30 pixel large spatial frequency range. Since their high-frequency components have been cut off uniformly, they appear like a bright-field illuminated image of low resolution.

FPI simulation results are listed for image sequences consisting of 9, 25, 49 and 81 LR images. Their step factor of successive LR images is 0.35. For comparison, first row shows the centered LR input images' bicubic interpolation. FPI results for USAF-1951 target show both, reconstructed HR Fourier spectrums and reconstructed HR amplitude images. For recovered slanted edge HR amplitude images, each MTF50P value is determined to compare resolution enhancement.

MTF50P value can be interpreted as a system-MTF (modulation transfer function). It outputs the spatial frequency response (SFR) in line pairs per millimeter (LP/mm) for a given contrast – here, a contrast of 50 % of its peak value (MTF50P) is considered. For determination, we use Burn's algorithm SFRMAT3 based on [18].

6. DISCUSSION

Adaption of classical FPI techniques to PMD cameras requires consideration of several aspects as discussed in chapter 3. These can be outlined in recording of macroscopic objects, differentiation of three different phase information types and appropriate choice of illumination. Experimental setup has to be in a reflective mode illumination as PMD cameras use their inherent light source to record amplitude and distance data. Furthermore, large pixel sizes limit lateral resolution and significantly reduce information density of captured object plane.

Aperture-scanning FPI enhances resolving power synthetically by capturing multiple intensity images. Each image transmits deviating spatial frequencies which could be imagined as changes from bright-field to dark-field illumination.

Simulations promise significant increase in resolution for PMD camera's amplitude images as shown in chapter 5. For evaluation we define LR input image's bicubic interpolation as a basis for comparison. In general, single-frame interpolation approaches increase resolution virtually by calculating additional sampling points between measured pixel values. No further object information is recorded and therefore the Fourier spectrum is strongly limited as can be seen in Figure 4. While low spatial frequencies are transmitted, high frequencies are still missing. As a result, letters of bicubic interpolated USAF-1951 target cannot be interpreted and measured spatial frequency response at MTF50P is only of 26 LP/mm. Instead, superposition of nine frequency domain-shifted LR input images according to FPI algorithm recovers higher spatial frequencies. Spatial frequency domain is expanded and the sample's HR amplitude output is recovered in more detail (see Figure 4, second row). Square shaped bandpass in Fourier domain is due to the sensor's low resolution. Its resolution is multiple times weaker than the lens' resolving power, so that the sensor's geometry represents the constraint in Fourier space. Combination of nine LR input images, each of different spatial frequency information, nearly doubles the optical system's resolving power. MTF50P is then increased to 49 LP/mm. This behavior continues for image sequences with more input images until the entire theoretical frequency bandpass of 120 x 120 pixels is recovered. For 49 and 81 LR input images resolving power is nearly tripled to a maximum of 73 LP/mm. Increase of lateral resolution enhancement via FPI follows an asymptotic progression.

In general, camera's maximum travel distance d_{max} and the number of input images limits resolution enhancement via aperture-scanning FPI. Firstly, the further the camera is moved, the

more diffraction orders are recorded. Light of narrow spectral bandwidth is diffracted more than light of wider spectral bandwidth and thus, favors increase of resolution. Light source's spectral bandwidth limits camera's maximum travel distance which provides additional object information. Secondly, number of input images depends on the optical system's NA that defines size of the bandpass constraint in Fourier domain. Minimum number of input images results from the overlap (> 60 %) of consecutive images and the size of Fourier space which needs to be reconstructed.

With spatial coherence provided, equation 8 illustrates dependence of light source's maximum allowable fractional disparity $\frac{\lambda_{min}}{\lambda_{max}}$ (as representative value for temporal coherence) as well as optical system's NA and focal length f'. Following trigonometric relationship exists where $\emptyset_{NA}$ is NA's diameter or width/ height respectively:

$$\frac{\sin(\tan^{-1}(d_{max}-\emptyset_{NA}/2)/f'))}{\sin(\tan^{-1}(d_{max}+\emptyset_{NA}/2)/f'))} = \frac{\lambda_{min}}{\lambda_{max}} \tag{8}$$

7. CONCLUSIONS

With this work, we have introduced FPI for 3D PMD cameras to overcome limited lateral resolution. It discusses the need of a reflective mode illumination which ends in a recommendation for an aperture-scanning setup. Corresponding simulations promise a significant increase in lateral resolution for low-resolution intensity images. Superimposing nine input images almost doubles the system's spatial resolution as higher frequent spatial content is recovered by FPI algorithm. Increasing number of input images improves resolving fine objects. It is apparent that resolution enhancement with FPI has an asymptotic behaviour reaching a synthetic resolution limit.

As an outlook, we first would like to confirm simulations described in this paper with real measurements. Then, possibilities of increasing PMD camera's depth resolution via FPI will be investigated. It will be evaluated if reconstructed phase provides additional information for depth's resolution enhancement and if FPI is able to increase depth resolution by superimposing individual phase images.

REFERENCES
[1] ifm electronic gmbh, *O3D303 data sheet.* [Online] Available: https://www.ifm.com/products/us/ds/O3D303.htm. Accessed on: Jul. 13 2017.
[2] G. Zheng, R. Horstmeyer, and C. Yang, "Wide-field, high-resolution Fourier ptychographic microscopy," (eng), *Nature photonics*, vol. 7, no. 9, pp. 739–745, 2013.
[3] R. Schwarte, "3D-Kamera nach Laufzeitverfahren," DE4439298 A1, Jun 13, 1996.
[4] R. Lange, "3D Time-of-flight distance measurement with custom solid-state image sensors in CMOS/CCD-technology," Dissertation, 2000.
[5] H. G. Heinol, "Untersuchung und Entwicklung von modulationslaufzeitbasierten 3D-Sichtsystemen," Dissertation, 2001.
[6] M. Lindner and A. Kolb, "Calibration of the intensity-related distance error of the PMD TOF-camera," *Proc. SPIE 6764, Intelligent Robots and Computer Vision XXV: Algorithms, Techniques, and Active Vision*, no. 6764W, 2007.
[7] M. Lindner, I. Schiller, A. Kolb, and R. Koch, "Time-of-Flight sensor calibration for accurate range sensing," *Computer Vision and Image Understanding*, vol. 114, no. 12, pp. 1318–1328, 2010.
[8] G. Zheng, *Fourier ptychographic imaging: A MATLAB tutorial,* 20160501st ed. San Rafael: Morgan & Claypool Publishers, 2016.

[9] S. Dong *et al.,* "Aperture-scanning Fourier ptychography for 3D refocusing and super-resolution macroscopic imaging," (eng), *Optics express*, vol. 22, no. 11, pp. 13586–13599, 2014.

[10] E. Kolenović, "Untersuchung zur Kopplung von Intensität und Phase in monochromatischem Licht," Dissertation, 2006.

[11] R. Gross, *Physik III - Optik und Quantenphänomene: Kapitel 7: Abbildungstheorie*. Vorlesungsskript zur Vorlesung WS 2002/2003. [Online] Available: https://www.wmi.badw.de/teaching/Lecturenotes/Physik3/Gross_Physik_III_Kap_7.pdf. Accessed on: Jul. 13 2017.

[12] S. Dong, Z. Bian, R. Shiradkar, and G. Zheng, "Sparsely sampled Fourier ptychography," (eng), *Optics express*, vol. 22, no. 5, pp. 5455–5464, 2014.

[13] L. Tian, X. Li, K. Ramchandran, and L. Waller, "Multiplexed coded illumination for Fourier Ptychography with an LED array microscope," (eng), *Biomedical optics express*, vol. 5, no. 7, pp. 2376–2389, 2014.

[14] H. Lietz and J. Eberhardt, "Contribution to the standardization of 3D measurements using a high-resolution PMD camera," *Proc. SPIE 9628, Optical Systems Design 2015: Optical Fabrication, Testing, and Metrology V*, no. 9628H, 2015.

[15] P. Burns and D. Williams, "Sampling efficiency in digital camera performance standards," *Proc. SPIE 6808, Image Quality and System Performance V*, no. 6808, 2008.

[16] J. D. van Ouwerkerk, "Image super-resolution survey," *Image and Vision Computing*, vol. 24, no. 10, pp. 1039–1052, 2006.

[17] K. Nasrollahi and T. B. Moeslund, "Super-resolution: A comprehensive survey," *Machine Vision and Applications*, vol. 25, no. 6, pp. 1423–1468, 2014.

[18] P. Burns, *sfrmat 2.0 User's Guide*. [Online] Available: http://read.pudn.com/downloads108/sourcecode/math/448322/sfrmat2_guide.pdf. Accessed on: Jul. 18 2017.

CONTACTS

Henrik Lietz   henrik.lietz@hs-weingarten.de
Prof. Dr. Jörg Eberhardt   joerg.eberhardt@hs-weingarten.de